PHILOSOPHICAL TRANSACTIONS OF THE ROYAL SOCIETY A MATHEMATICAL, PHYSICAL & ENGINEERING SCIENCES

Strain and Stress Analyses from Calcite Twin Lamellae in Experimental Buckles and Faulted Drape-Folds

M. Friedman, L. W. Teufel and J. D. Morse

Phil. Trans. R. Soc. Lond. A 1976 **283**, 87-107
doi: 10.1098/rsta.1976.0071

Phil. Trans. R. Soc. Lond. A. **283**, 87–107 (1976) [87]
Printed in Great Britain

Strain and stress analyses from calcite twin lamellae in experimental buckles and faulted drape-folds†

By M. Friedman, L. W. Teufel and J. D. Morse
Center for Tectonophysics, Texas A & M University, College Station, Texas, 77843, U.S.A.

Studies of calcite twin lamellae in an experimental thick-beam fold, a multilithologic, layered thin-beam buckle, and in several multilithologic faulted and drape-folded specimens provide a test of the use of these lamellae to map the strain and stress fields developed under known, yet complex, boundary conditions. Even though the number of grains available for sampling per domain of homogeneous deformation is small (8 to 100), we find that in 24 of 28 domains studied the derived orientations and relative magnitudes of the principal strain axes agree to $\pm 30°$ with the corresponding inferred principal stress axes, with those inferred from accompanying microfractures and faults, and with those expected from the bending and the boundary conditions. The absolute differences in strain between those inferred from the twin lamellae and those calculated from bedding-thickness changes or from the surface strains recovered from distorted grid-lines averages ± 0.01. The poorest correlations are for domains where the sample size is < 20. In addition, the twin-lamellae strain analyses permit better definitions of superposed deformation and anticlastic bending than do the corresponding stress analyses. For strains up to about 0.15, calcite twin lamellae are remarkably good indicators of the strain and stress histories of deformations.

Introduction

Dynamic petrofabric studies are made with a view toward inferring (*a*) the orientations and relative magnitudes of the principal stresses and strains throughout the deformational history of a rock, and (*b*) the absolute, or at least, the relative magnitudes of the physical parameters existent during deformation, especially: the effective confining pressure, differential stress, temperature, and strain-rate. Calcite twin lamellae are perhaps the most useful of all fabric elements in this regard because from their development and orientation one can infer the orientation and relative magnitude of the principal stresses (Turner 1953), principal strains (Groshong 1972, 1974), differential stress (Jamison 1974; Jamison & Spang 1974), principal stress ratios (Friedman & Heard 1974), and the brittle versus ductile behaviour of the material (Donath *et al.* 1971; Tobin & Donath 1971). The methods yielding information on the orientation and relative magnitudes of principal stresses have been tested adequately through study of experimentally and naturally deformed rocks (Friedman 1963, 1964; Carter & Friedman 1965; Carter & Raleigh 1969; Friedman & Stearns 1971; among many others). Here we are concerned primarily with correlations between principal stresses and strains determined from calcite twin lamellae, and between the corresponding strain magnitudes and those calculated from length changes in experimentally produced folds.

The experimentally folded thick beams (Handin *et al.* 1972), multilithologic thin beams (Pattison 1972; Handin *et al.*, in the press), and drape-folds (Friedman *et al.* 1972, 1973, and in

† Part V of the series Experimental folding of rocks under confining pressure, Center for Tectonophysics, Texas A & M University.

the press; Min 1974) provide an excellent opportunity to test the reliability of twin lamellae as a dynamic tool, not just in axially symmetric, deformed right-cylinders (as in most previous experimental work), but in rock deformed dry, at 100 MPa confining pressure and under known, yet complex, boundary conditions that produce superposed deformations and inhomogeneous stress fields. In this report, calcite data for the buckled thick- and thin-beam folds and for the drape folds are presented in more detail than in the corresponding general reports (Handin *et al.* 1972; Pattison 1972; and Friedman *et al.*, in the press). The purpose here is to emphasize the calcite data rather than the folding, faulting, and microfracturing, with a view toward demonstrating the usefulness of twin lamellae in the solution of structural problems.

Specifically, for a thick beam fold of Lueders Limestone, strains are calculated from the twin lamellae and are compared with surface strains determined from distortion of a grid pattern inked on the specimen before folding and with the pattern of compression and extension axes also inferred from the twin lamellae. Then, for a five-layer multilithologic, thin-beam specimen the strains from the calcite are correlated with the corresponding stress axes. It will be shown that the internal agreement for the calcite data in these unstable folds is excellent. Calcite data for two faulted drape-fold specimens include compression and extension axes patterns and strain calculated from twin lamellae and from bedding thickness changes.

In this paper compressive stresses and shortening strains are counted positive, tensions and elongations are negative. The greatest principal compressive stress is σ_1; σ_2 is the intermediate, and σ_3 is the least compressive. Principal strain axes ϵ_1, ϵ_2 and ϵ_3 stand for the greatest, intermediate and least shortenings, respectively. Strain magnitudes are expressed in absolute values and as percentages, i.e. strain of 0.01 is equal to 1 %.

Starting materials

The thick-beam fold is of Lueders Limestone (Permian, north-central Texas), a fine-grained, greyish-tan, and macroscopically homogeneous and isotropic rock. It is composed almost exclusively of calcium carbonate in the form of micrite, diagenetically altered organic particles, echinoid fragments, sparry calcite-cement and fossil-fillings. Only the sparry calcite is sufficiently coarse grained for optical study (mean size about 0.1 mm). The starting material contains essentially no twin lamellae, and the calcite crystals are randomly oriented dimensionally and crystallographically. Although the porosity is about 17 %, the void spaces are small and appear to be distributed mainly in the micrite. That is, few twin lamellae occur in the sparry calcite as a result of pore space collapse upon application of confining pressure and differential stress.

The limestone in the thin-beam fold and in the faulted-drape folds is the Indiana (Mississippian, Bedford, Indiana). It is a medium-grained, greyish, and macroscopically homogeneous rock composed of calcium carbonate in the form of oolites, diagenetically altered organic particles, echinoid, crinoid, and other fossil fragments, and abundant sparry calcite-cement and fossil-fillings. Bedding is manifest in thin section by dimensional alignment of fossils. The amount of micrite is smaller and the size of the sparry crystals is larger (about 0.3 mm) than in the Lueders Limestone. Calcite crystals in the starting block are essentially untwinned, and they are also randomly oriented crystallographically. Porosity ranges from 10 to 20 % with pore space distributed such that some twin gliding upon pore collapse cannot be excluded.

Methods

General

Ideally, twin lamellae, being planar features, should be studied in three mutually perpendicular thin sections to eliminate partial sampling. This was done for the thick-beam fold of Lueders Limestone, but it was not possible for the thin-beam fold or for the faulted drape-folds because in these specimens the size of the domains of reasonably homogeneous deformation are too small. Data from the thin-beam fold are obtained from one section cut perpendicular to the fold axis; those from the drape folds come either from one or two parallel sections (both cut perpendicular to the fold axis) or from two perpendicular sections, the second cut parallel to the fold axis. Exactly similar results from the two perpendicular sections, e.g. specimen 298, indicate that little significant data are lost if only one section is used.

All measurements are made with the universal-stage. Compression and extension axes are inferred from the best developed set of twin lamellae in each grain after Turner (1953, 1961). Measurements of bedding thickness and lengths of grid lines from which strains are calculated are made with calibrated eyepiece micrometer and are accurate to better than 0.01 mm. The techniques for obtaining strains from twin lamellae is new and for convenience is described briefly below.

Strain from twin lamellae

Strain measurement techniques based upon the mechanical twinning of calcite have evolved from the work of Conel (1962), Spang & Chapple (1969, 1970), and Groshong (1972, 1974). The least-squares, strain gauge technique of Groshong (1972, 1974) is used here because it successfully avoids certain anomalous results inherent in Conel's and Spang & Chapple's methods (Groshong 1972). The amount of shear strain in a given twin set Γ is a function of its orientation relative to the principal strain axes. The transformation equation (1), relates the shear strain Γ to the components

$$\begin{aligned}\Gamma = {} & l_1 l_2 \epsilon_x + m_1 m_2 \epsilon_y + n_1 n_2 \epsilon_z + (l_1 m_2 + m_1 l_2)\Gamma_{xy} \\ & (m_1 n_2 + m_2 n_1)\Gamma_{yz} \\ & (n_1 l_2 + l_1 n_2)\Gamma_{zx}\end{aligned} \tag{1}$$

of the strain tensor (Jaeger & Cook 1969, p. 44). The quantities l_1, m_1, n_1, l_2, m_2 and n_2 are the direction cosines which relate the normal to the twin plane and the glide direction, respectively, to thin section coordinates. Groshong (1972), describes methods for computing these by vector algebra from the orientations of the pole to the twin set and the optic axis. According to Conel (1962, pp. 57–58) Γ is:

$$\Gamma = \tfrac{1}{2}\gamma = \tfrac{1}{2}\tan\psi = \frac{0.347}{t}\sum_{i=1}^{n} t_i \tag{2}$$

where γ is the engineering shear strain, ψ the angular shear (which is fixed in calcite twin gliding), t the thickness of the grain normal to the twin set, n the number of twins in the set, and t_i the thickness of the individual twin. Since twin gliding is a constant volume process, and cannot be used to measure bulk volume changes, an assumption of zero volume change is made, hence:

$$\epsilon_x + \epsilon_y + \epsilon_z = 0 \quad \epsilon_z = -(\epsilon_x + \epsilon_y). \tag{3}$$

Substitution of equation (3) into equation (1) gives

$$\begin{aligned} \Gamma = {} & (l_1 l_2 - n_1 n_2)\,\epsilon_x + (m_1 m_2 - n_1 n_2)\,\epsilon_y \\ & + (l_1 m_2 + m_1 l_2)\Gamma_{xy} \\ & + (m_1 n_2 + n_1 m_2)\Gamma_{yz} \\ & + (n_1 l_2 + l_1 n_2)\Gamma_{zx}, \end{aligned} \tag{4}$$

a linear equation in five unknowns. Thus, measurement of the requisite crystallographic elements in five twin sets will yield a system of five equations of the form (4) which could then be solved simultaneously to yield the components of strain. The third normal strain is computed from equation (3), and the principal strains are then calculated. In practice more than five twin sets are used in order to minimize the effect of observational errors and heterogeneity, and to provide an estimate of the precision of the analysis. The $n > 5$ equations of the form (4) resulting from such measurements constitute a system which, in the general case, has no exact solution. However, a best-fit strain tensor may be computed from the data using the method of least-squares (multiple linear regression) Groshong (1972).

From the least-squares strain tensor an expected shear strain for each twin set can be calculated. Because twin gliding in calcite occurs only with a positive sense of shear, all of the expected shear strains should be positive for a single homogeneous deformation. As Groshong (1974) points out, a negative shear strain indicates the host grain was not properly oriented for twin gliding with respect to the computed strain tensor. A few small negative values might occur if the least-squares solution has a large standard error, or if the deformation is not exactly homogeneous, but many and large negative values indicate either gross heterogeneity or multiple homogeneous deformations during which twin gliding occurs with respect to two or more different stress systems. In this study and in Teufel (1975) we demonstrate that separate analysis of twin sets with positive and negative expected shear strains permits recognition of polyphase deformation.

In practice, all twin sets are measured in every grain and each twin set is treated independently. Thick-twin, thickness measurements are made using the inner thickness of the twin. A twin lamella too thin to exhibit the twinned structure between composition planes appears as a black line across the grain. The thickness of each such 'microtwin' is fixed at 0.5 μm of twin per micrometre of black line (Groshong 1974). In our material all twin lamellae are extremely thin and are treated as 'microtwins'. Where possible a minimum of 50 grains were measured for each domain. This was not always possible in the drape folds since the domains of reasonably homogeneous deformation are too small.

In study of natural folds the least-squares, strain gauge technique has yielded principal strain orientations and relative magnitudes that are consistent with those expected from bending of isotropic layers, but the magnitudes are usually too small (Spang & Chapple 1969, 1970; Groshong 1971*a*, *b*; Teufel & Groshong 1973; Chapple & Spang 1974). However, Groshong (1973, 1974) found a close fit between the principal strain and the measured axial shortenings in a suite of eight experimentally deformed cylinders of Indiana Limestone shortened to 0.085 (8.5 %). The average difference between axial strain measured experimentally and that calculated from the twin lamellae is 0.01 while the directions of ϵ_1 and σ_1 across the boundaries of the cylinder agree to within an average of 7°. Accordingly, the small strains observed in natural folds may be real and due to folding mechanisms other than twin gliding such as bedding-plane-slip as suggested by Chapple & Spang (1974).

PHILOSOPHICAL TRANSACTIONS OF THE ROYAL SOCIETY A MATHEMATICAL, PHYSICAL & ENGINEERING SCIENCES

Computer usage

The calcite strain and stress analyses reported here were completed with the aid of FORTRAN IV programs written for an IBM 360/65 computer. One program (requiring 200 K bytes storage) written by Dr R. H. Groshong calculates the best-fit strain tensor in thin section coordinates by multiple linear regression, and gives the statistics necessary to estimate the precision of the analysis. It also transforms this tensor into principal coordinates and computes strain tensors by the methods of Conel (1962) and Spang & Chapple (1969). Another program (requiring 50 K bytes storage) developed in the Center for Tectonophysics calculates compression and extension axes, rotates them into any plane of reference (after McIntyre 1963), and plots and contours them (on the line printer) in number of points per 1 % area.

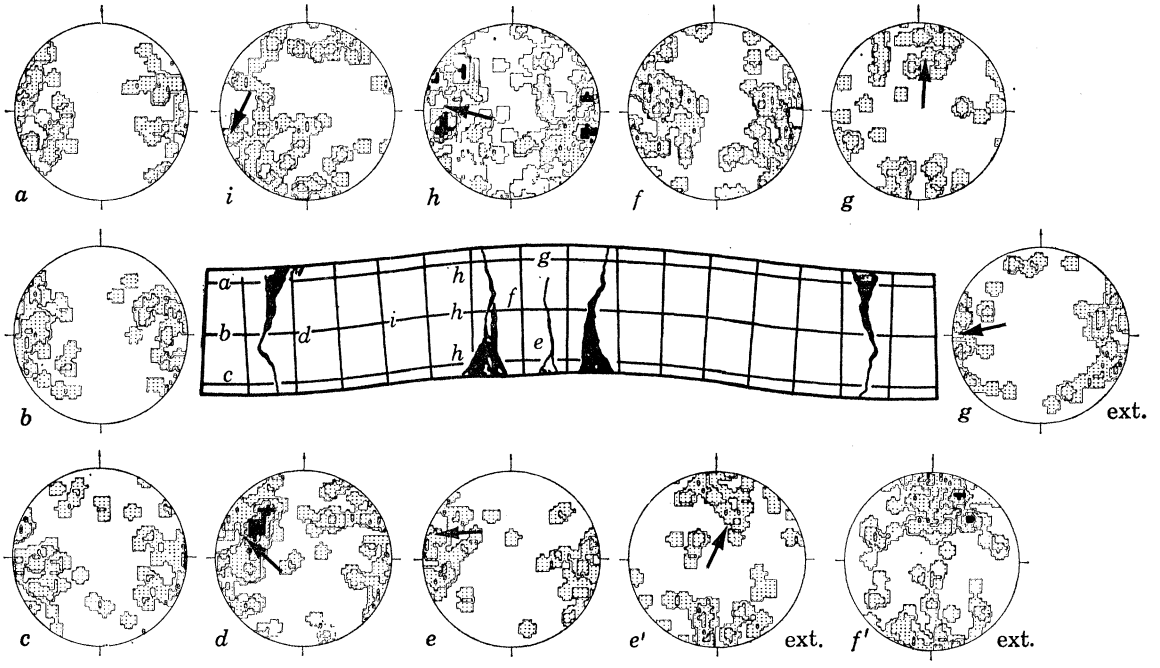

FIGURE 1. Calcite compression and extension axes at nine locations (*a*–*g*) on *XY* surface of specimen 14. The plane of each diagram is parallel to the *XY* surface and perpendicular to the fold axes. Diagrams *a*–*i* are of 50, 50, 50, 100, 48, 86, 48, 142 and 62 compression axes, respectively; and diagrams *e*′–*g*′ are of 48, 86 and 50 extension axes, respectively. Contours are at 1, 2, 4 and 6 points per 1 % area. Arrows in diagrams *d*, *e*, *i*, *h* and *g* indicate orientation of ϵ_1 and those in diagrams *e*′ and *g*′ the orientation of ϵ_3. Strain axes determined from calcite twin lamellae.

RESULTS

Thick-beam fold

The fold of Lueders Limestone is specimen 14 initially described by Handin *et al.* (1972, Table 1, Figures 16, 17, 19 and 20). The specimen (initially 20 cm long and 3.2 cm in width and height) was shortened 9.2 % at 100 MPa confining pressure, at a shortening rate of 10^{-4}/s, dry, and at 24 °C. Fold deflexion is 0.5 cm and maximum limb dip is 5° (figure 1). The original data on orientations of principal stress axes (derived from the calcite twin lamellae) and on the surface strains (calculated from distorted grid lines) are repeated here to facilitate comparison with new data on the state of strain determined from the twin lamellae.

Stress axes

Compression and extension axes derived from calcite e_1 lamellae were determined at 16 localities in specimen 14 (figures 1 and 2). In order to correlate exactly the fabric data with specimen location it is necessary to illustrate the data from single thin sections cut perpendicular and parallel to the hinge.

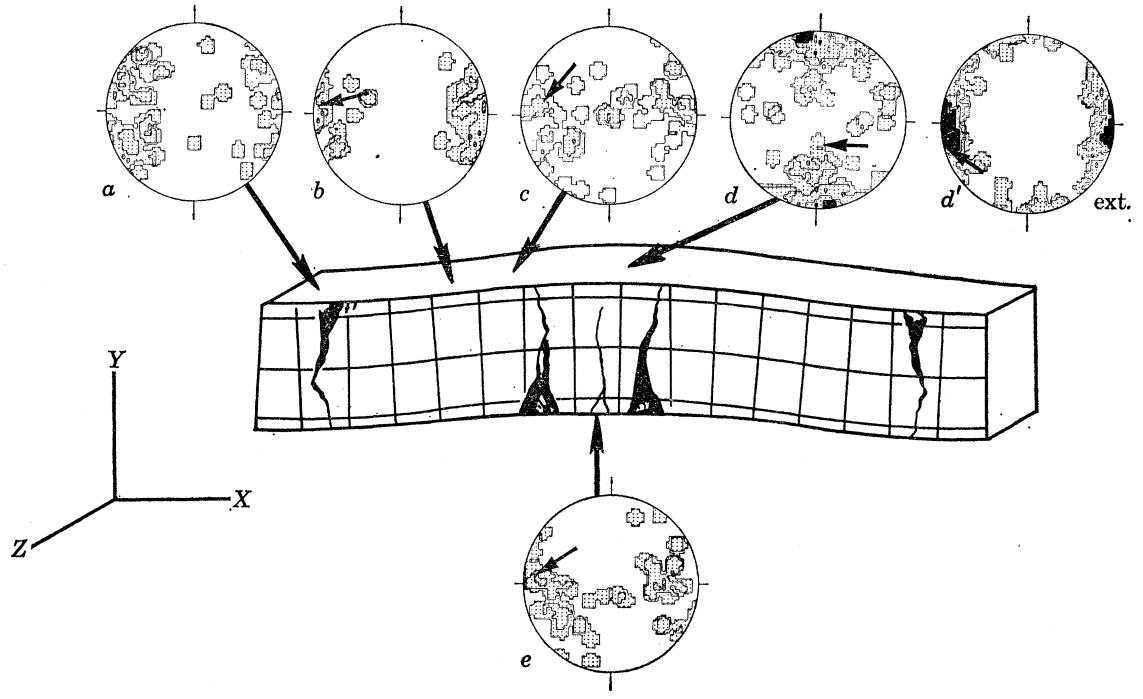

FIGURE 2. Calcite compression and extension axes at five locations (*a–e*) on *XZ* surface specimen 14. Plane of each diagram is parallel to the *XZ* surface of the fold; the fold axes are indicated by the fine arrows (north–south). Diagrams *a–e* are of 50, 36, 49, 88 and 49 compression axes, respectively; and diagram *d′* contains 38 extension axes. Contours are at 1, 2, 4 and 6 points per 1% area. Arrows on diagrams *b–e* indicate ϵ_1 and that on *d′* indicates ϵ_3.

For the surface perpendicular to the hinge (figure 1) several trends repeatedly occur, as follows:

1. At localities *a*, *b* and *c* the compression axes are concentrated subparallel to the direction of axial shortening, which is east–west on the diagram.
2. At *d* the compression axes are noticeably skewed to the horizontal axis.
3. At locality *i* in the inflexion region the compression axes are more widely scattered than they are elsewhere.
4. At locality *g* the compression axes are rotated 90°, and they are grouped perpendicular to the hinge and the uppermost surface of the fold, i.e. north–south on the diagram.
5. Comparison of the patterns for localities *f* and *g* shows that in *f* there is a minor north–south concentration of compression axes whereas in *g* there is a minor east–west concentration. Clearly, these patterns define the cross-over between the compressive and extensile regions in the beam.

6. Typical extension axes distributions are illustrated at three localities (figure 1). The axes fall into partial or complete girdles oriented 90° to the corresponding patterns of the compression axes.

For the XZ surfaces (figure 2) the patterns of the stress axes show the following trends.

1. In the trough of the syncline (locations a and b) and at the lowermost fibre of the anticline (location e) the compression axes are grouped parallel to the direction of axial shortening (X).

2. In the inflexion region (location c) the compression axes form a girdle around the fold axis (Z).

3. At the crest of the anticline (location d) at the uppermost fibre the compression axes are strongly oriented parallel to the fold axis. A composite diagram at a and d (from figures 1 and 2, respectively) yields a girdle parallel to the axial plane (YZ) of the anticline. Minor concentrations in both d and g are oriented east–west, parallel to the direction of axial shortening.

4. The extension axes at d' show a strong orientation parallel to the direction of axial shortening. The pattern at d agrees with the extension axes at nearby location g' (figure 1). Extension axes at location e (not illustrated) from a uniform girdle parallel to the axial plane of the anticline.

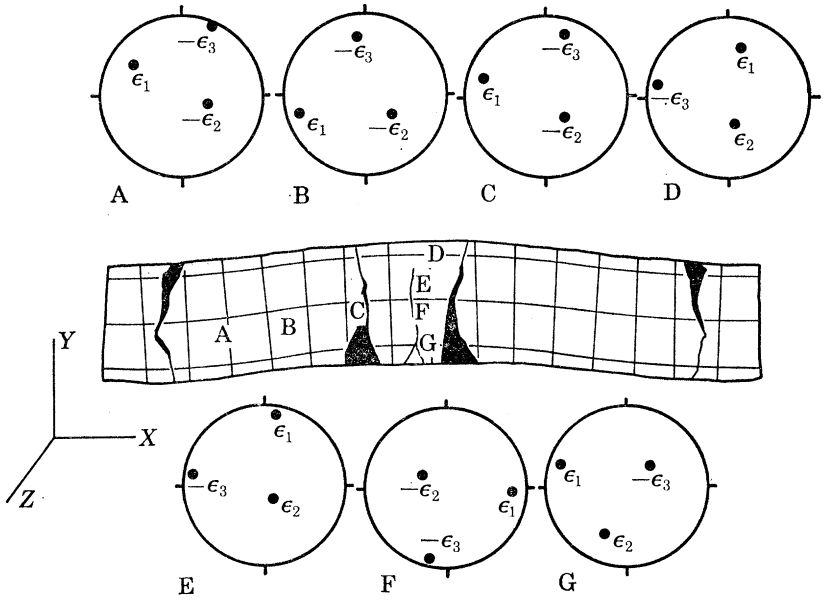

FIGURE 3. Diagrams show orientations of principal strain axes determined from twin lamellae at location A–G, specimen 14. Data are plotted in lower hemisphere, equal-area protection with plane of each diagram parallel to XY surface. Fold axis is at the centre of each diagram. ϵ_1 is the axis of greatest shortening, ϵ_2 the axis of intermediate strain, and ϵ_3 the axis of least shortening, shortenings are counted positive.

Strains from calcite twin lamellae

The three dimensional state of strain is determined from the calcite twin lamellae at eleven locations in the fold. These data consist of the orientations and magnitudes of principal strain axes (figures 3 and 4, table 1), and the strains parallel to X, Y and Z (table 1).

The orientations of the principal strain axes are in excellent agreement with those of the principal stresses (compare figures 1 and 3, 2 and 4). At localities B, C, G and F, all in the lower (compressional) part of the beam, the axis of greatest shortening ϵ_1 is subparallel to X (figure 3).

At locality A, ϵ_1 is skewed to X in exactly the same sense and amount as the corresponding compressional stresses (figure 1*d*). A traverse up the trace of the anticlinal axial plane shows a 90° change in ϵ_1 between E and F reflecting the change associated with crossing a neutral point in the fold. At E and D the greatest elongation ϵ_3 is subparallel to X and ϵ_1 is inclined at low angles to Y. Similar changes are shown at locations H–K (figure 4). Specific correlation of ϵ_1 with the pattern of compression axes at each location is shown by the short arrow (ϵ_1) on figures 1 and 2.

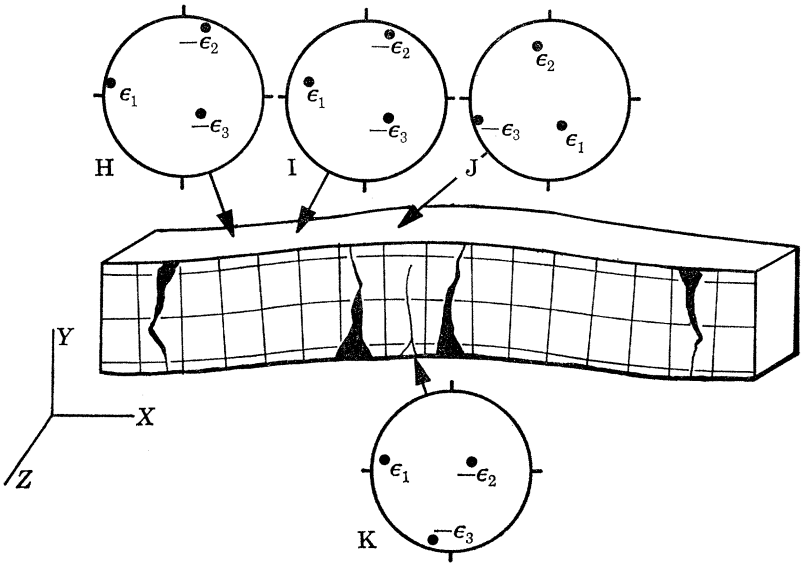

FIGURE 4. Diagrams show orientations of principal strain axes determined from twin lamellae at locations H–K, on the *XZ* surface of specimen 14. Data are plotted in lower hemisphere, equal-area projection with plane of each diagram parallel to the *XZ* surface. Fold axis is north–south.

TABLE 1. STRAIN DATA FROM CALCITE TWIN LAMELLAE, THICK-BEAM FOLD, LUEDERS LIMESTONE

location	no. of grains	strain magnitudes† ϵ_1	ϵ_2	ϵ_3	ϵ_x	ϵ_y	ϵ_z
XY surface							
A‡	53	0.045	−0.011	−0.034	0.043 ± 0.024§	−0.023 ± 0.012	−0.020 ± 0.011
B	51	0.043	−0.008	−0.035	0.041 ± 0.021	−0.032 ± 0.019	−0.009 ± 0.007
C	54	0.038	−0.004	−0.034	0.042 ± 0.019	−0.022 ± 0.012	−0.020 ± 0.016
D	52	0.028	0.005	−0.033	−0.034 ± 0.018	0.011 ± 0.006	0.023 ± 0.013
E	43	0.022	0.001	−0.023	0.022 ± 0.010	−0.023 ± 0.009	0.001 ± 0.001
F	38	0.042	−0.011	−0.031	0.040 ± 0.020	−0.032 ± 0.018	−0.008 ± 0.008
G	51	0.095	0.035	−0.130	0.085 ± 0.048	−0.059 ± 0.038	−0.144 ± 0.086
XZ surface							
H‡‡	54	0.043	−0.012	−0.031	0.038 ± 0.018	−0.020 ± 0.016	−0.018 ± 0.010
I	53	0.028	−0.012	−0.016	0.010 ± 0.005	−0.004 ± 0.003	−0.006 ± 0.004
J	54	0.024	0.004	−0.028	0.022 ± 0.021	−0.011 ± 0.006	−0.021 ± 0.014
K	52	0.125	−0.014	−0.111	0.110 ± 0.057	0.009 ± 0.002	−0.119 ± 0.052

† Sign convention: shortenings are counted positive, elongations are negative.
‡ See figure 3 for sampling localities.
§ Plus or minus values are the standard errors.
‡‡ See figure 4 for sampling localities.

The principal strains vary in magnitude (table 1) also as anticipated from simple 'beam theory'. For example, ϵ_1 ($\approx \epsilon_x$) is greatest at locations K and G (0.125 and 0.095, respectively) in the lowermost portion of the anticlinal hinge, i.e. in the zone where compression in the X-direction due to bending is superposed on compression parallel to X caused by end-loading the specimen. Maximum elongations also occur at G and K where elongation is maximum parallel to the fold axis due to anticlastic bending (discussed below).

Strain magnitudes along the anticlinal axial plane parallel to Z, i.e. parallel to the fold axis, are especially noteworthy (figure 5). ϵ_z is a shortening of 0.02 at the top and an extension of -0.12 at the bottom. The point of zero strain, approximately one-third the way down from the uppermost fibre coincides with the cross-over from extension to compression reflected in the principal stresses (figure 1, *f*–*g*) and strains (figure 3, F–E). The strain plan reflected in ϵ_z (figure 5) is a well known phenomenon and has been termed 'anticlastic bending' (Ramsay 1967, p. 402) or the familiar 'rubber eraser' effect.

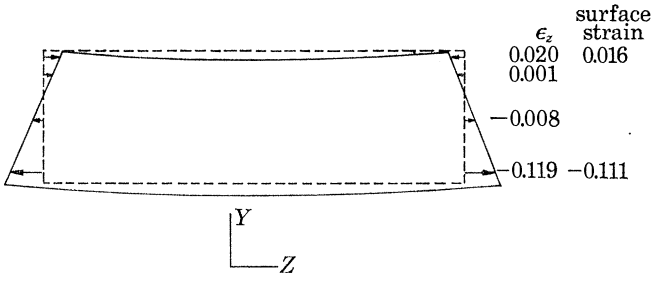

FIGURE 5. Sketch of anticlastic bending shows distortions of specimen along axial plane of anticline (YZ), specimen 14. Strains parallel to ϵ_z are listed as determined from calcite twin lamellae (left column) and from distorted grid (right column). Cross-over between contraction and extension parallel to ϵ_z correlates with region between localities *f* and *g* (figure 1).

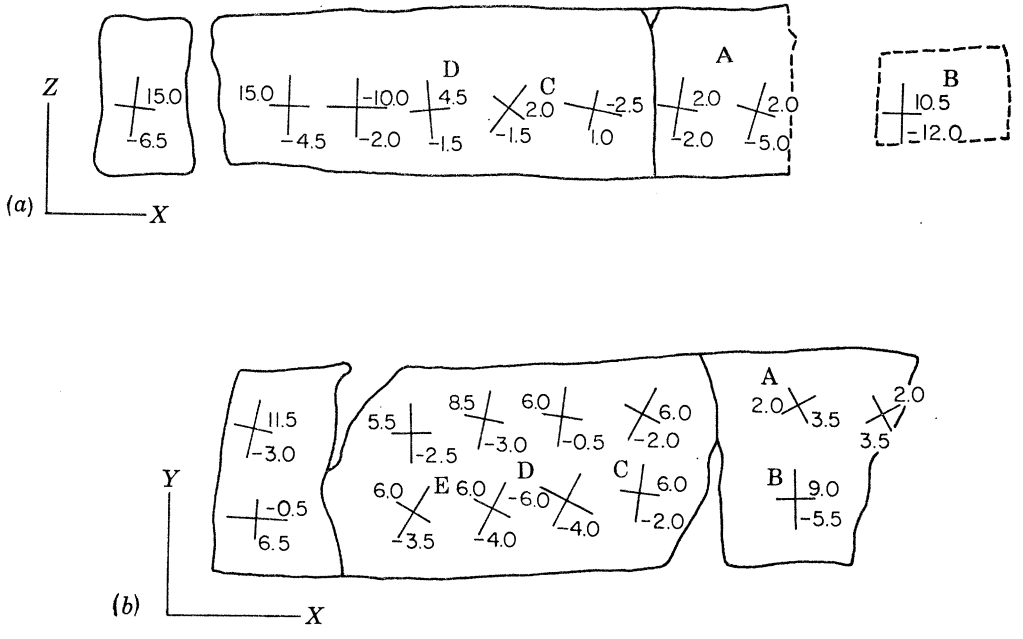

FIGURE 6. Secondary principal strains as determined from distorted grid pattern on the XZ and XY surfaces of specimen 14 (*a* and *b*, respectively). Shortenings are counted positive; strain magnitudes are percentages, e.g. 11.5% is 0.115. Localities A–D (*a*) and A–E (*b*) refer to table 2 (column 1).

Surface strains

Strains at the surface of the specimen are calculated from measurements of the distortions of an original square grid (1.2 cm) marked before deformation. Each cell is treated as a 45° rosette, the means of the two parallel sides and of the diagonals form the three-gauge configuration. The strain for each gauge is the original length minus the final length divided by the original length (shortenings counted as positive), and the secondary principal strains are the major and minor axes of the ellipse calculated from these three strains. Calculations are based on the not entirely realistic assumptions that the state of strain within each cell is homogeneous, the original dimensions of all the cells are identical, no displacements are due to fracturing, and that the strains are small.

A map of the secondary principal strains along two faces of half of specimen 14 (figure 6) shows that the orientations of the surface strains agree with those from the calcite twin lamellae and the corresponding stress axes. The strains are symmetrically disposed on the other half of the specimen (Handin *et al.* 1967, Fig. 17). Along the uppermost fibre of the *XZ* plane (figure 6*a*) the principal compressive (+) and extensile (−) strain axes at the left end of the specimen (adjacent to the piston) are perpendicular and parallel, respectively, to the synclinal fold axis (figure 6*a*). These axes progressively rotate toward the right until at the anticlinal crest they are reversed; i.e. the maximum shortening is subparallel to the fold axis. Along the opposite parallel surface at the lowermost fibre, the strains are the reverse of those along the uppermost fibre as indicated at locality B. On the *XY* surface, i.e. perpendicular to the fold axes (figure 6*b*), the strains reflect the zones of compression and extension associated with the synclinal and anticlinal axes, and show the progressive changes expected from bending stresses (Currie *et al.* 1962; Dieterich & Carter 1969; Dieterich 1970; Friedman & Sowers 1970). For example, high in the synclinal fold (at left end of specimen) the principal strain subparallel to *X* is compressive while low in the fold it is extensile. Conversely, near the anticlinal hinge, the principal strain subparallel to *X* shows a large shortening (9 %) low in the fold. Strains along the flank show progressive corresponding changes and rotations.

Comparison of strain magnitudes

Strains parallel to *X*, *Y* and *Z* as determined from the distorted grids (surface strains) are compared to those determined from the twin lamellae at eighteen corresponding locations (table 2). The maximum absolute difference between corresponding strains is 0.022 and the average difference is only 0.007 (standard deviation is 0.007). Percent differences are large for certain domains (maximum of 43 %, average of 20 %) because the strains themselves are small with regard to the average difference of 0.007. Some of the differences in strain magnitudes no doubt arise from errors inherent in each technique. Another source, however, arises from the fact that the thin sections from which the twin lamellae are measured come from locations that are not at the specimen surface. That is, since the strains demonstrably vary from domain to domain some variation in magnitude is to be expected over the distance of a few millimetres that might separate a given grain from the adjacent specimen surface. Supporting this view are the facts that the thin sections parallel to the *XZ* surface were all cut within 4.0 mm of the surface containing the grid cells and that the corresponding strains for this surface are in better agreement than are those for the *XY* surface where the twin lamellae are located at greater distance from the specimen surface (table 2). Considering what might be true strain variation

between the surfaces and the thin sections, the agreement (within 0.01) between surface strains and those calculated from calcite twin lamellae is remarkably good.

Thin-beam fold

Stress and strain axes

Strains and compression axes from calcite twin lamellae are determined at three localities along the anticlinal, axial plane of the five-layer, thin beam, Indiana Limestone – Coconino Sandstone – specimen no. 152 (figure 7). The directions of ϵ_1 tend to change from layer to layer with the pattern of compression axes; the latter were derived earlier at the same locations (Pattison 1972). Broadly viewed, both sets of axes show changes expected from bending of an isotropic beam. This interpretation is supported by the microfracture development which indicates that the cross-over from the zone of compression to that of extension occurs in the middle of the lower sandstone layer (Pattison 1972, Fig. 18, p. 54). In all three domains the compression axes seem to define the bending stresses somewhat better than do the strain axes with the angle between ϵ_1 and the mean σ_1 about 30–40°. In each domain the principal strain axes are not perpendicular or parallel to the layering, but occupy intermediate orientations. This perhaps reflects the net strain resulting from superposition of strains associated with buckling the layers and the strains resulting from anticlastic bending (figure 5). Further supporting this view is the fact that the strains parallel to the fold axis ϵ_z at locations A, B and C clearly reflect the anticlastic bending, and those normal to bedding (ϵ_y) do not show the thickening and thinning of the layers expected from simple bending theory (table 3).

TABLE 2. COMPARISON OF SURFACE STRAINS AND THOSE CALCULATED FROM CALCITE TWIN LAMELLAE

XZ surface		surface strain	difference	percent difference
	E_x			
A†	−0.032	−0.047	0.015	32
B	0.110	0.111	0.001	1
C	0.010	0.008	0.002	25
D	0.038	0.039	0.001	2
	E_z			
A	0.021	0.016	0.005	31
B	−0.119	−0.111	0.008	1
C	−0.006	−0.008	0.002	25
D	−0.018	−0.016	0.002	12
XY surface				
	E_x			
A‡	−0.034	−0.031	0.003	9
B	0.085	0.063	0.022	26
C	0.042	0.062	0.020	32
D	0.041	0.055	0.014	26
E	0.042	0.039	0.004	10
	E_y			
A	0.011	0.008	0.003	37
B	−0.059	−0.055	0.004	7
C	−0.022	−0.023	0.001	4
D	−0.032	−0.024	0.008	33
E	−0.023	−0.016	0.007	43

† See figure 6*a* for sampling localities.
‡ See figure 6*b* for sampling localities.

PHILOSOPHICAL TRANSACTIONS OF THE ROYAL SOCIETY A MATHEMATICAL, PHYSICAL & ENGINEERING SCIENCES

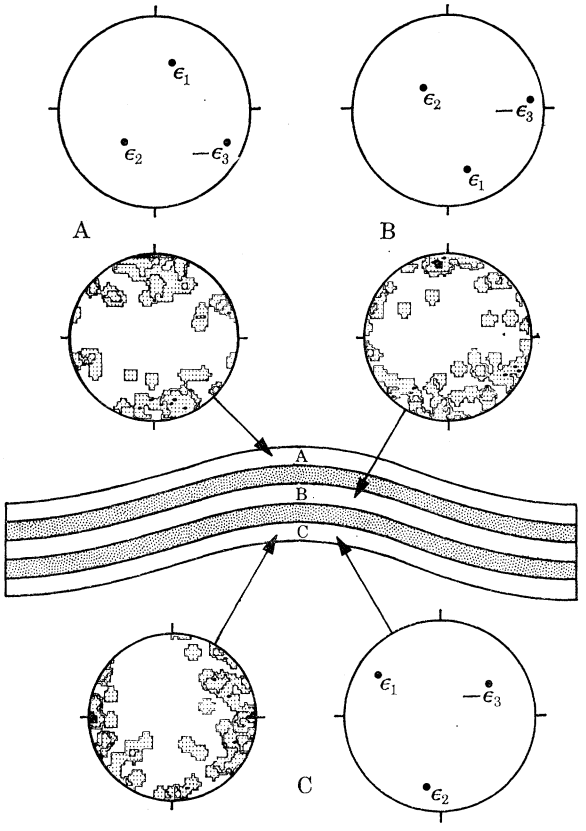

FIGURE 7. Diagrams illustrate orientations of principal strain axes and of compression axes (contoured) determined from calcite twin lamellae at localities A, B and C in specimen 152. Specimen is an unstable fold of three limestone layers (A, B and C) and two intervening sandstone layers (stippled). Data are plotted in lower hemisphere, equal-area projection with the plane of each diagram oriented perpendicular to the fold axis. Contoured diagrams contain 50 compression axes each with contours at 1, 2 and > 4 points per 1% area (after Pattison 1972, figure 11D, E, F). Strain analyses are based on 33, 37 and 42 sets of twin lamellae for A, B and C, respectively. Magnitudes are listed in table 3.

TABLE 3. STRAIN MAGNITUDES, SPECIMEN 152 – THIN-BEAM BUCKLE

location†	no. of twins	Strains					
		ϵ_1	ϵ_2	ϵ_3	ϵ_x‡	ϵ_y	ϵ_z
A	33	0.030	0.002	−0.032	−0.032 ± 0.014§	0.029 ± 0.015	0.003 ± 0.001
B	37	0.023	0.002	−0.025	−0.024 ± 0.009	0.020 ± 0.010	0.004 ± 0.002
C	42	0.088	0.011	−0.099	0.088 ± 0.042	0.010 ± 0.005	−0.099 ± 0.047

† See figure 7 for sampling localities.
‡ *X*, *Y* and *Z* oriented relative to axial plane as in figure 2, i.e. *X* is perpendicular to axial plane, *Z* is parallel to the fold axis, and *Y* is perpendicular to layering.
§ Plus or minus values are the standard errors.

Strain magnitudes

The magnitudes of the strains reflect in part the superposition of bending and end-loading. For examples, ϵ_x (oriented parallel to layering and normal to fold axis) is extensive in layers A and B and compressive in layer C. Maximum layer thinning occurs at A (compare values for ϵ_y). The layers are compressed parallel to the fold axes (ϵ_z) at A and B, and extended in this direction at C, i.e. the anticlastic bending effect mentioned above. For this specimen it is not

possible to compare directly ϵ_y with the strains normal to layering as determined from layer thickness changes because plucking of grains near the top and bottom boundaries during thin section preparation prohibits accurate measurement of layer thickness.

Faulted drape-folds

Introduction

Faulted drape-folds are produced experimentally by forcing a 'basement' block of sandstone (2 by 3 by 12.6 cm) along a lubricated pre-cut surface or 'reverse fault' into an intact 'sedimentary veneer' consisting of from 1 to 5 layers of limestone and sandstone, at confining pressure to 200 MPa, shortening rates of 10^{-3}–10^{-6} s^{-1}, and room temperature (figure 8*a*, *b*).

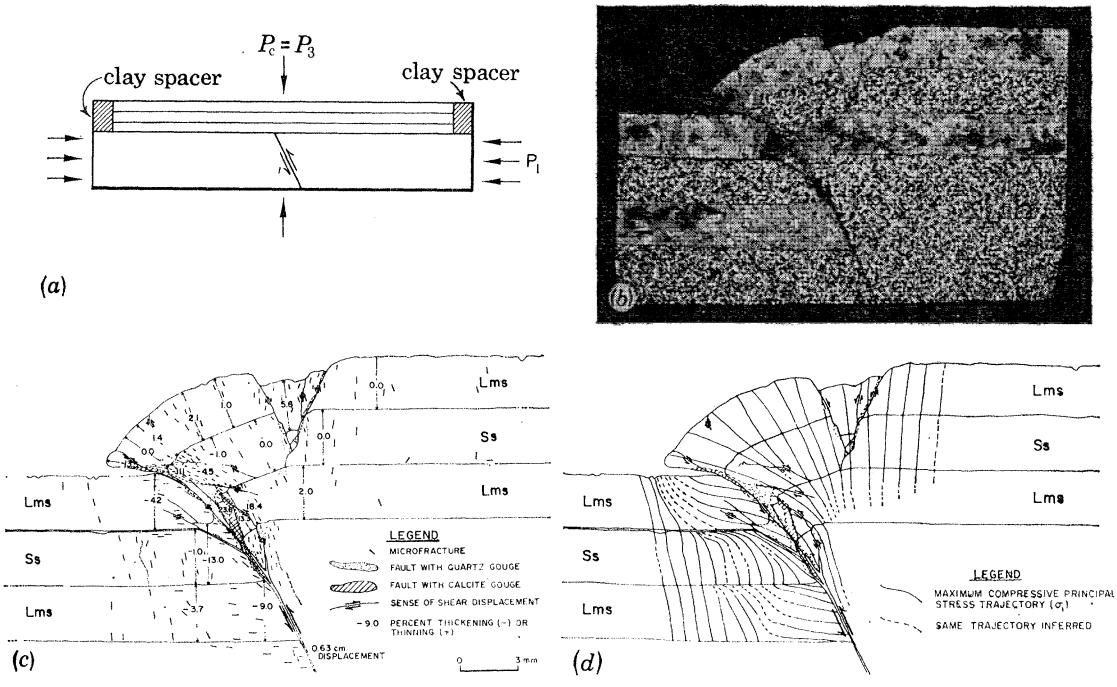

FIGURE 8. Faulted drape-folds. (*a*) Schematic diagram of loading condition for three layers deformed over a 65° lubricated pre-cut in the forcing member. (*b*) Photomicrograph of specimen 298 shows upthrown forcing block on right with overlying graben in uppermost limestone layer, curving upthrust, and thickened downthrown layers. (*c*) Map of faults and microfractures in specimen 298, also shows strains (percentages) perpendicular to layering as calculated from layer thickness changes, thinnings are positive. (*d*) Stress trajectories inferred from faults, microfractures, and calcite data, specimen 298.

Details of the experimental procedure are given by Friedman *et al.* (in the press) along with description of faults, bedding thickness changes, senses of bedding plane slip, hinges, gouge zones, microfractures and some aspects of the calcite fabrics, and correlation between stress trajectories inferred from the deformation features and those calculated from numerical modelling (also see Min 1974). The orientations of principal stresses derived from microfractures, faults, and calcite twin lamellae are in excellent agreement among themselves and with the calculated ones (figure 8*c* and *d*). Here we will treat in detail only with the calcite fabrics in two specimens (nos. 298 and 295).

In hindsight the Indiana Limestone is somewhat unsatisfactory owing to its high porosity (10–20 %) and large mean grain size (about 0.3 mm). Initial collapse of pores under confining

pressure and further collapse during deformation probably generates twin-lamellae in adjacent grains. These are unavoidably sampled during analysis, and contribute scatter to the data, i.e. add to the apparent heterogeneity of the stress and strain fields. The large grain size causes a problem because the domains in which the deformation is statistically homogeneous are themselves small. Accordingly, sample population per domain is smaller (20–40) than desirable even though data are obtained from several parallel thin sections for some specimens. Most of the results come from studies of thin sections cut perpendicular to fold axes. However, examination of mutually perpendicular thin sections from specimen 298 (second section cut parallel to the fold axis) reveals that no significant data are lost through use of a single section.

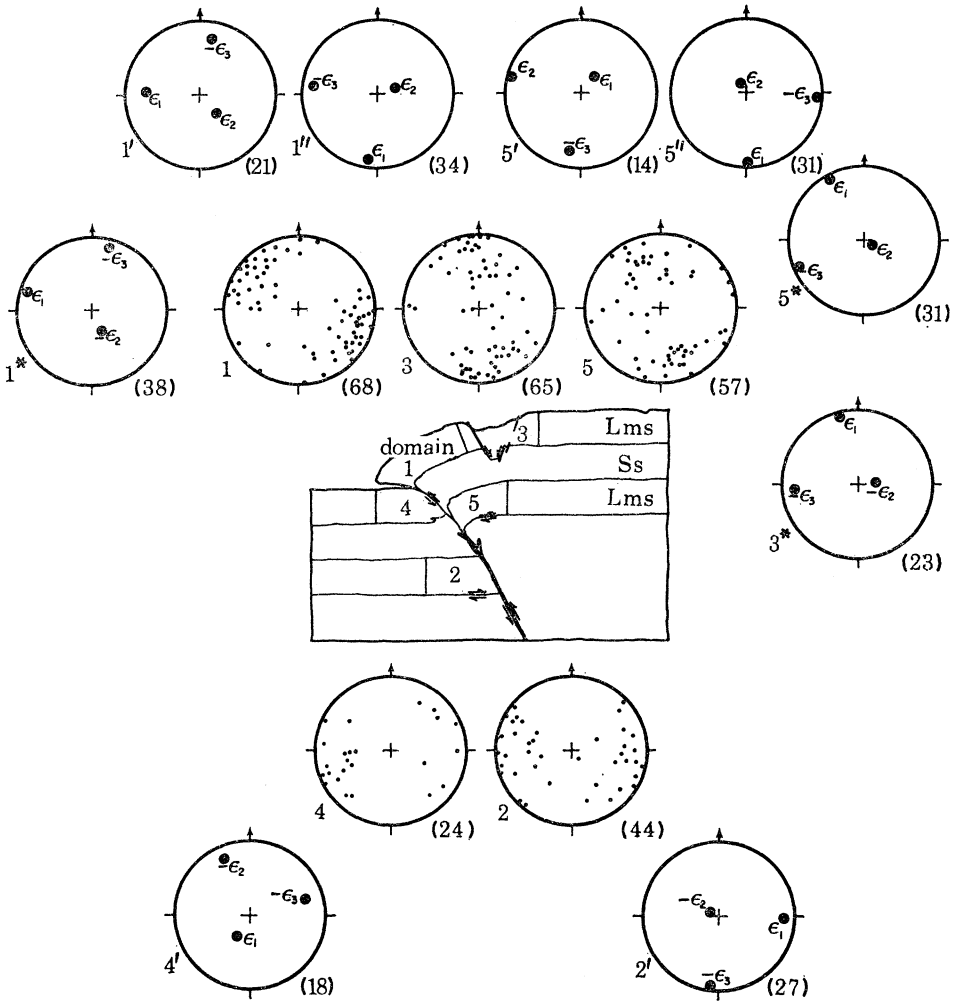

FIGURE 9. Diagrams illustrate orientation of compression axes and principal strain axes determined from calcite twin lamellae in domains 1–5, specimen 298. Data are plotted in lower hemisphere equal area projection; plane of each diagram is perpendicular to fold axis. Number of sets of e_1 twin lamellae from which data are obtained is given in parentheses for each diagram, and the numbers 1–5 correspond to domains 1 through 5. Compression axes are shown in diagrams 1 through 5. Principal strain axes are shown in diagrams with superscript symbols. Diagrams 1′, 1″ and 5′, 5″ represent two different solutions based on segregated data in domains 1 and 5, respectively (see text). Diagrams 1*, 3* and 5* represent strain analyses from thin sections cut parallel to fold axis; otherwise data are from sections cut perpendicular to fold axis.

PHILOSOPHICAL TRANSACTIONS OF THE ROYAL SOCIETY A MATHEMATICAL, PHYSICAL & ENGINEERING SCIENCES

Stress axes

Compression and extension axes are inferred from calcite twin-lamellae in seven specimens. The relatively small numbers of calcite grains per domain somewhat limits the power of this tool; nevertheless, certain significant trends are readily apparent. The data for specimens 298 and 295 are illustrated (figures 9 and 10, respectively) because the numbers of data points are the largest available. As in many previous studies (e.g. Friedman 1963; Carter & Friedman 1965; Handin *et al.* 1972), the patterns of compression axes adequately show the significant trends.

In specimen 298 the compression axes exhibit a definite, non-random pattern in each of the five domains (figure 9). In the downthrown block, domains 2 and 4, the maximum principal compressive stress σ_1 inferred from each point diagram is subparallel to the layering. The pattern shifts 90° in domains 3 and 5 of the upthrown block where compression axes are distributed along broad, great-circle girdles with many axes inclined at 60–90° to the layering. Thus the layer-parallel σ_1 in the downthrown block and the layer-parallel extension of the upthrown block, including the graben formation, are clearly reflected in the distributions of compression axes. In domain 1 the pattern is again rotated, reflecting both the dip of the extended layer (axes nearly normal to bedding) and possibly the horizontal orientation of σ_1 associated with the thrust fault. That is, domain 1 is not one of homogeneous, single-phase

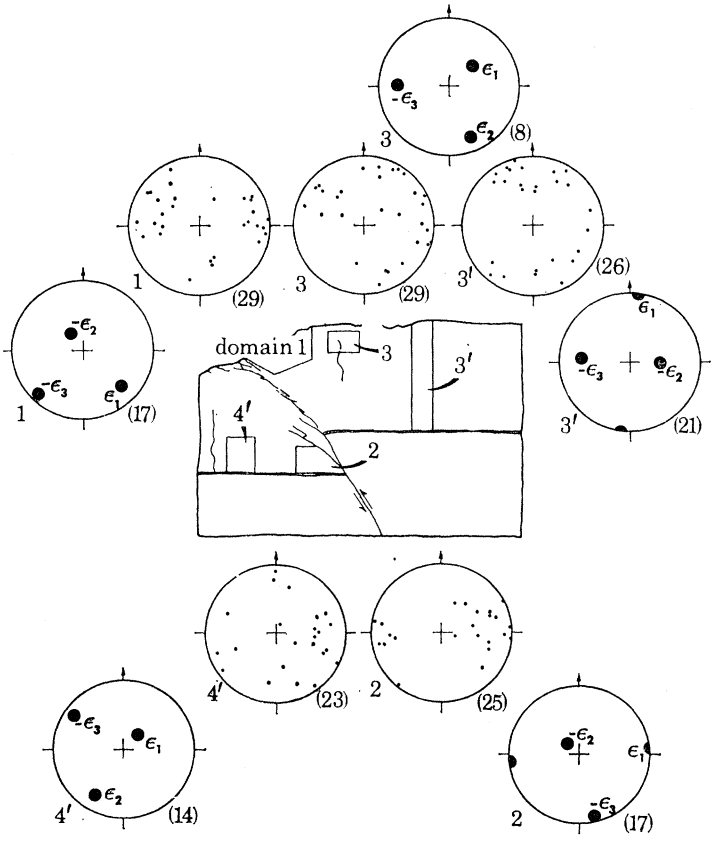

FIGURE 10. Diagrams illustrate orientations of compression axes and principal strain axes as determined from calcite twin lamellae in domains 1–4, specimen 295. See caption figure 9 for explanation.

deformation. A second suggestion of superposed deformation is evident in domains 3 and 5 where compression axes are at low angles to the fold axis as well as at high angles to the layering. It will be shown later that these patterns agree with the strain analyses of calcite twin-lamellae and the strains calculated from bedding thickness changes. Also the orientations of micro-fractures in this specimen are in good agreement with the calcite compression axes (cf. figures 8*c* and 9).

Similar patterns are recorded for specimen 295 (figure 10). Domains in the downthrown block (2 and 4) show compression axes that reflect a layer-parallel σ_1. In the upthrown block (figure 10, domain 3′) axes are inclined at high angles to bedding which reflect the layer-parallel extension of these layers. In specimen 295, domain 1 also seems to show compression axes related to both the thrust faults and to curvature of the layer. The compression-axis patterns in domain 3, specimen 295, are poorly defined.

TABLE 4. STRAINS CALCULATED FROM CALCITE TWIN-LAMELLAE, COMPARED WITH THOSE FROM LAYER-THICKNESS CHANGES, SPECIMEN 298

domain number	average strain from layer-thickness change	principal strains from calcite twin-lamellae ϵ_1	ϵ_2	ϵ_3	strain normal to layering calcite twin-lamellae	no. of twin sets in the analysis	difference in strains normal to bedding (col. 2–col. 6)
1	0.021†	0.022	0.004	−0.026	0.016	55	0.005
2	−0.037	0.035	−0.008	−0.028	−0.023	28	−0.014
3	0.056‡	0.030	0.001	−0.041	0.014	19	0.042‡
3§	0.056‡	0.036	−0.001	−0.026	0.016	23	0.040‡
4	−0.042	0.081	−0.038	−0.043	−0.019	18	−0.023
5	0.020	0.041	0.001	−0.052	−0.036	60	−0.016
5§	−0.020	0.039	0.018	−0.056	0.017	31	0.003

† Shortenings (e.g. layer thinning) are counted positive.
‡ Value is probably too large because material at top of graben was lost in preparation of thin section.
§ From thin section cut parallel to fold axis. Other data are from thin sections cut perpendicular to fold axis.

Strain axes

The orientations of the principal strain axes and their magnitudes as determined from the twin lamellae vary among domains just as do the inferred stresses (figures 9, 10, table 4). In specimen 298, the principal strain axes agree with the stress axes in domain 2, but disagree in domain 4 (figure 9). For domain 1 and 5 more than a third of the measured twin sets have negative expected shear strains. By segregating the data on the basis of positive and negative shear strains two sets of principal strain axes (diagrams 1′ and 5′ versus 1″ and 5″) are recognized for each domain. In domain 1, the two sets of principal strains reflect the nearby thrust fault (i.e. ϵ_1, the axis of maximum shortening, is nearly horizontal, diagram 1′) and the thinning of the layer (i.e. ϵ_1 is normal to and ϵ_3 parallel to the layering, diagram 1″). Further, calcite crystals located close to the fault yield the data in diagram 1′. In domain 5, the thinning of the layer is indicated (diagrams 5″ and 5*) while a shortening parallel to the fold axis is suggested (diagram 5′). In domain 3, ϵ_1 is also normal to the layers, and ϵ_3 is horizontal in agreement with the strain plan of layer-thinning and graben-formation. For domains 1 and 5, there is good agreement in the strains determined from the two perpendicular thin sections. In general the strain magnitudes are less than 5 % (table 4). Strains calculated normal to the layering from

the calcite twin-lamellae and from layer-thickness changes differ on the average by only 0.01 (table 4, uncertain values for domain 3 omitted).

In specimen 295, the principal strain axes agree with the pattern of compression axes in domains 2 and 3′ where the latter are well defined (figure 10). In domain 2, ϵ_1 is parallel to the layer boundary, and ϵ_3 is normal to it; in domain 3′, the axes are rotated 90° so that ϵ_1 is normal, and ϵ_3 is parallel to the layering. These are identical to the strain patterns in similarly located domains in specimen 298 (cf. figures 9 and 10). In domains 3 and 4′ the compression axes are scattered; but the principal strains are consistantly oriented even though they are calculated from only 8 and 14 sets of lamellae, respectively. In each domain the axis of greatest shortening is inclined at low angles to the fold axis. Shortening parallel to the fold axis is also recognized from the strain analysis of the thick-beam fold of Lueders Limestone, and it is suggested also in specimen 298 (figure 9, domain 5′). Perhaps 'anticlastic' bending, is operative in the drape-folding as well as in the unstable folding. Principal strains throughout specimen 295 are less than 3 %. Correlation with layer-thickness change in this specimen is impossible because the domains are too small compared to the layer thickness.

Strain magnitudes

Strain magnitudes derived from calcite twin lamellae and their correlation with strain calculated from bedding thickness changes are given for each of the five domains in specimen 298 (table 4). These data correspond to the solutions for the principal strains in each domain shown in figure 9. The difference between the strains calculated normal to bedding from the two techniques average 0.01 (average of 2 strain differences, table 4, col. 8), moreover, the two sets of strains for each domain are the same sign, i.e. the beds are thickened in domains 2 and 4 and are thinned elsewhere. The magnitudes of ϵ_1, ϵ_2 and ϵ_3 in each domain vary little (0.022 to 0.041, -0.008 to 0.018 and -0.026 to -0.056, respectively) except in domain 4 where ϵ_1 and ϵ_2 are anomously large. Perhaps this anomaly arises because the sample size (18 sets of twin lamellae) is relatively small. It is also in domain 4 that the directions of ϵ_1 and σ_1 disagree the most (figure 9).

Discussion

Strain analyses

Study of the experimentally folded thick beam, multilithologic thin beam, and the faulted drape-folds provide good tests of the accuracy and reliability of Groshong's (1972, 1974) method of strain analysis from calcite twin-lamellae. In these materials the internal strain and stress fields are complex, superposed deformations occur in certain domains, and there are independent internal checks on strain magnitudes (bedding thickness changes or distorted grid lines) and on the direction and relative magnitudes of the principal stresses (calcite twin-lamellae and microfractures). The fundamental limitation of the work is the relatively small number of grains (8–100) per domain available to sample. Nonetheless, in most domains there is remarkably good agreement between the stresses and strains. For example, consider the correlations between the directions of the principal stresses and strains. Although, in principle, the corresponding axes of stress and strain are not necessarily parallel for inelastic deformations, large angular differences do not occur for small strains. We find that in a total of 28 domains investigated (figures 1, 2, 3, 4, 7, 9 and 10) ϵ_1 in 20 domains is oriented within 30° of σ_1 derived from the calcite twin-lamellae. Furthermore, in 4 of the 8 domains where the angular difference is

$> 30°$, the strain axes are oriented in mechanically significant directions not reflected in the derived principal stresses (e.g. figures 9 and 10, domain 4). In the main, domains in which the strains do not track the stresses are those for which the sample size for strain analysis is small (< 20).

The strain analyses of the twin lamellae appears to be more adept than the stress technique in helping to identify superposed deformations. For example, in domain 1 of specimen 298 (figure 9) stresses related to the thrust fault are superposed on those due to bending. The distribution of compression axes derived from the calcite twin-lamellae centres about an intermediate orientation, while sub-samples from the strain analysis clearly show two distinct orientations of ϵ_1. The basis for sub-sampling is not subjective; the sense of shear for twin gliding is fixed and when a calculated shear strain of the wrong sign arises from the twin-lamellae data for a given grain it suggests either inhomogeneous deformation or superposed deformation (Groshong 1974). This occurrence in a few grains suggests the former, an abundance of them indicates superposed deformation where the individual stress states vary widely in orientation. When this occurs, results such as those in figure 10 are obtained by recalculating the principal strains from each group of data.

The fact that only the average orientations of ϵ_1, ϵ_2 and ϵ_3 are plotted for each domain (e.g. figures 3, 4, 9, etc.) gives the false impression that these axes are more precisely defined than are the corresponding stress axes. It should be realized that the strain axes are calculated from a least-squares solution of the strain components contributed from all the grains sampled. A measure of the actual dispersion about the average orientations is given by the standard error (see, for example, table 3).

Perhaps even more impressive is the comparison of strain magnitudes between those calculated from the twin lamellae and those from bedding thickness changes or surface strains from distorted grid lines. For examples: In the thick-beam fold, surface strains are compared to those calculated from twin lamellae. The maximum absolute difference between corresponding strains is 0.022 and the average difference is only 0.007 with a standard deviation of 0.007 (table 2). In faulted-drape fold no. 298, comparisons are made with bedding thickness changes, and in five instances where comparisons are justified, the maximum absolute strain difference is 0.023, and the average is 0.01 (table 4). The correlation between strain to 0.01 is exactly the same as that between axial shortening measured experimentally and the corresponding strains determined from the twin lamellae in a suite of experimentally deformed cylinders of Indiana Limestone (Groshong 1973, 1974).

Stress analysis

The use of compression and extension axes derived from calcite twin-lamellae (after Turner 1953) to position the orientations and relative magnitudes of the principal stress axes in the rock at the time of twin gliding is well known. In all the experimentally folded specimens we find, a reasonably good fit in the orientation patterns for these axes with the stresses inferred from microfractures and with the expected stress fields in such structures as derived from elastic or viscoelastic solutions (Currie *et al.* 1962; Dieterich & Carter 1969; Friedman & Sowers 1970; and Min 1974). It is important to recognize that the compression or extension axes tend to be grouped broadly on petrofabric diagrams, and that precise definition of the orientation of a given principal stress axis is statistical at best. Commonly the statement 'σ_1 is oriented subparallel to bedding and normal to the fold axis' really means the stress axis is positioned within $\pm 30°$. Accordingly, one speaks of the statistical centre of the grouping or mean vector (Ramsay

1967, p. 15). What is important, however, is the obvious and significant changes in orientation of the patterns of axes from one domain to the other (e.g. figures 1, 2, 7 or 9). These leave little doubt in the validity of the interpretation. Specific comments which may be useful to those who apply this technique are stated elsewhere (Turner 1953, 1961; Friedman 1964, 1967; Handin *et al.* 1972).

Anticlastic bending

When beams or plates are bent the outer fibres of the fold tend to contract parallel to the fold axis and the lower fibres tend to expand in this direction (figure 5). This behaviour has been termed anticlastic bending by engineers and Ramsay (1967, p. 402), and is also referred to commonly as the 'rubber-eraser' effect. The strain analysis of the thick-beam fold clearly demonstrates that this Poisson effect is manifest in the permanent deformation of the fold, and gives rise to strains as large as 0.12 (figure 5). The corresponding stress field is partly reflected in the pattern of compression axes (figure 2, diagram *d*), and in the pattern of shear fractures developed high in the fold, which reflect σ_1 parallel to the fold axis (Handin *et al.* 1962, Fig. 13*b*, *c*). In addition aspects of anticlastic bending are apparent in the strain analyses of the faulted-drape folds (e.g. figure 9, diagrams 4′ and 5′; figure 10, diagram 4′).

One can only speculate on how important anticlastic bending is in nature. Usually the effect is recognized when beams or plates of limited width are bent, whereas in the field, folds occur in plates of considerable dimension parallel to the fold axis. It is fact, however, that fracture patterns reflecting σ_1 parallel to the fold axis and others showing σ_3 parallel to the fold axis at the time of fracture are common in folded strata (Stearns 1968; Friedman & Stearns 1971; etc.). It remains for future study to determine whether anticlastic bending produces permanent deformation in naturally folded rocks.

Conclusions

From this study of calcite twin-lamellae in three types of experimentally produced folds, the following conclusions seem warranted, namely:

The method for determining strain magnitudes and directions from calcite twin-lamellae that has evolved from the work of Conel (1962), Spang & Chapple (1969) and finally of Groshong (1972, 1974) is remarkably accurate ($\leqslant \pm 0.01$, i.e. 1 % strain) for strains up to about 0.15.

The strain analysis complements the stress analysis (after Turner 1953), and when used together they permit sufficient definition of the stress and strain fields, including superposed deformation, to help unravel the deformational history and describe it in mechanical terms.

Thus for strains up to about 0.15 at least, calcite twin-lamellae are remarkably good indicators of the strain and stress histories of deformations. The successful use of calcite twin-lamellae in dynamic petrofabric analyses represents one of the many contributions to structural geology that has come from programs of experimental rock deformation.

The authors wish to thank Dr J. Handin for his review of the manuscript, Dr K. D. Min for the experimentally deformed specimens, and a number of graduate students in Dr Friedman's course in structural petrology for their help in the fabric analyses. Our research on folding has been generously supported by the National Science Foundation, Grant DES74-22954.

PHILOSOPHICAL TRANSACTIONS OF THE ROYAL SOCIETY A MATHEMATICAL, PHYSICAL & ENGINEERING SCIENCES

References (Friedman *et al.*)

Carter, N. L. & Friedman, M. 1965 Dynamic analysis of deformed quartz and calcite from the Dry Creek Ridge Anticline, Montana. *Am. J. Sci.* **263**, 747–785.

Carter, N. L. & Raleigh, C. B. 1969 Principal stress directions from plastic flow in crystals. *Geol. Soc. Am. Bull.* **80**, 1231–1264.

Chapple, W. M. & Spang, J. H. 1974 Significance of layer-parallel slip during folding of layered sedimentary rocks. *Geol. Soc. Am. Bull.* **85**, 1523–1534.

Conel, J. E. 1962 *Studies of the development of fabrics in naturally deformed limestones*. Ph.D. Thesis, Dept. of Geology, Calif. Inst. Tech.

Currie, J. B., Patnode, H. W. & Trump, R. P. 1962 Development of folds in sedimentary strata. *Geol. Soc. Am. Bull.* **73**, 655–674.

Dieterich, J. H. 1970 Computer experiments on mechanics of finite amplitude folds. *Can. J. Earth Sci.* **7**, 467–476.

Dieterich, J. H. & Carter, N. L. 1969 Stress-history of folding. *Am. J. Sci.* **267**, 129–254.

Donath, F. A., Faill, R. T. & Tobin, D. G. 1971 Deformational mode fields in experimentally deformed rock. *Geol. Soc. Am. Bull.* **82**, 1441–1462.

Friedman, M. 1963 Petrofabric analysis of experimentally deformed calcite-cemented sandstones. *J. Geol.* **71**, 12–37.

Friedman, M. 1964 Petrofabric techniques for the determination of principal stress directions in rocks. In *State of stress in the Earth's crust* (ed. W. R. Judd), pp. 451–552. New York: American Elsevier Pub. Co. Inc.

Friedman, M. 1967 Description of rocks and rock masses with a view toward their mechanical behavior. *Proc. First Int. Cong. on Rock Mech., Lisbon, Portugal*, **III**, 182–197.

Friedman, M. & Sowers, G. M. 1970 Petrofabrics – A critical review. *Can. J. Earth Sci.* **7**, 477–497.

Friedman, M. & Stearns, D. W. 1971 Relations between stresses derived from calcite twin lamellae and macrofractures, Teton Anticline, Montana. *Geol. Soc. Am. Bull.* **82**, 3151–3162.

Friedman, M., Logan, J. M., Handin, J. & Stearns, D. W. 1972 Experimental 'drape-folding' of rocks under confining pressure (abstract). *Geol. Soc. Am. Abst. with Programs* **4**, 512–513.

Friedman, M., Logan, J. M. & Min, K. D. 1973 Petrofabric analysis of experimental drape folds and upthrusts (abstract). *Eos Trans A.G.U.* **54**, 458.

Friedman, M. & Heard, H. C. 1974 Principal stress ratios in Cretaceous Limestones from the Texas Gulf Coast. *Am. Ass. Petrol. Geol. Bull.* **58**, 71–78.

Friedman, M., Handin, J., Logan, J. M., Min, K. D. & Stearns, D. W. 1976 Experimental folding of rocks under confining pressure: Part III. Faulted drape-folds in multilithologic layered specimens. *Geol. Soc. Am. Bull.* **87**, in press.

Groshong, R. H. Jr. 1971*a* *Strain in minor folds, valley and ridge province, Pennsylvania*. Ph.D. Thesis, Dept. of Geology, Brown Univ. 223 p.

Groshong, R. H. Jr. 1971*b* Strain in natural single-layer folds (abstract). *Eos Trans A.G.U.* **52**, 345.

Groshong, R. H. Jr. 1972 Strain calculated from twinning in calcite. *Geol. Soc. Am. Bull.* **83**, 2025–2038.

Groshong, R. H. Jr. 1973 Experimental test of calcite strain-gage calculations (abstract). *Eos Trans A.G.U.* **54**, 458.

Groshong, R. H. Jr. 1974 Experimental test of least-square strain gage calculation using twinned calcite. *Geol. Soc. Am. Bull.* **85**, 1855–1864.

Handin, J., Friedman, M., Logan, J. M., Pattison, L. J. & Swolfs, H. S. 1972 Experimental folding of rocks under confining pressure: Part I. Buckling of single-layer rock beams. *Am. Geophys. Union Monograph* **16**, 1–28.

Handin, J., Friedman, M., Min, K. D. & Pattison, L. J. 1976 Experimental folding of rocks under confining pressure: Part II. Buckling of multilayered rock beams. *Geol. Soc. Am. Bull.* **87**, in press.

Jaeger, J. C. & Cook, N. G. W. 1969 *Fundamentals of rock mechanics*. London: Methuen & Co.

Jamison, W. R. 1974 *Numerical dynamic analysis of the McConnell thrust plate and associated structures*. M.S. Thesis, Dept. of Geology, University of Calgary, 98 p.

Jamison, W. R. & Spang, J. H. 1974 Determination of differential stresses in naturally deformed rocks (abstract). *Eos Trans A.G.U.* **55**, 433.

McIntyre, D. B. 1963 *Rotation of spherical projections*. Tech. Rep. No. 7, Dept. of Geology, Pomona College, Claremont, California, 10 p.

Min, K. D. 1974 *Analytical and petrofabric studies of experimental faulted drape-folds in layered rock specimens*. Ph.D. Dissertation, Dept. of Geophysics, Texas A & M University, December 1974, 90 p.

Pattison, L. J. 1972 *Petrofabric analysis of experimentally folded multilayered rocks*. M.S. Thesis, Dept. of Geology, Texas A & M University. August 1972, 71 p.

Ramsay, J. G. 1967 *Folding and fracturing of rocks*. New York: McGraw-Hill.

Spang, J. H. & Chapple, W. M. 1969 Twinning strain measurements from a naturally folded limestone (abstract). *Geol. Soc. Am. Abs. with Programs* **1**, 210–211.

PHILOSOPHICAL TRANSACTIONS OF THE ROYAL SOCIETY A MATHEMATICAL, PHYSICAL & ENGINEERING SCIENCES

Spang, J. H. & Chapple, W. M. 1970 Mechanical origin of folds in sedimentary rocks. A comparison between theory and observation (abstract). *Geol. Soc. Am. Abs. with Programs* **2**, 754–755.

Stearns, D. W. 1968 Certain aspects of fracture in naturally deformed rocks. In *Rock mechanics seminar* (ed. R. E. Riecker). Terrestrial Sci. Lab. Air Force Cambridge Res. Labs. Hanscom Field, Bedford, Mass., Clearinghouse for Fed. Sci. and Tech., AD669375, I, 97–118.

Teufel, L. W. 1975 Strain analysis of twinned calcite for two experimentally superposed deformations of Indiana Limestone (abstract). *Geol. Soc. Am. Abstracts with Programs*, 7, South-Central Section Mtg. Austin, Texas, 13–14 March, 1975.

Teufel, L. W. & Groshong, R. H. Jr. 1973 Strain analysis of twinned calcite in a naturally-deformed limestone mudcrack column (abstract). *Eos Trans. A.G.U.* **54**, 457.

Tobin, D. G. & Donath, F. A. 1971 Microscopic criteria for defining deformational modes in rock. *Geol. Soc. Am. Bull.* **82**, 1463–1476.

Turner, F. J. 1953 Nature and dynamic interpretation of deformation lamellae in calcite of three marbles. *Am. J. Sci.* **215**, 276–298.

Turner, F. J. 1961 'Compression' and 'tension' axes deduced from {01$\bar{1}$2} twinning in calcite (abstract). *Am. Geophys. Union Prog.* First Western Meeting, 55.

PHILOSOPHICAL TRANSACTIONS OF THE ROYAL SOCIETY A MATHEMATICAL, PHYSICAL & ENGINEERING SCIENCES

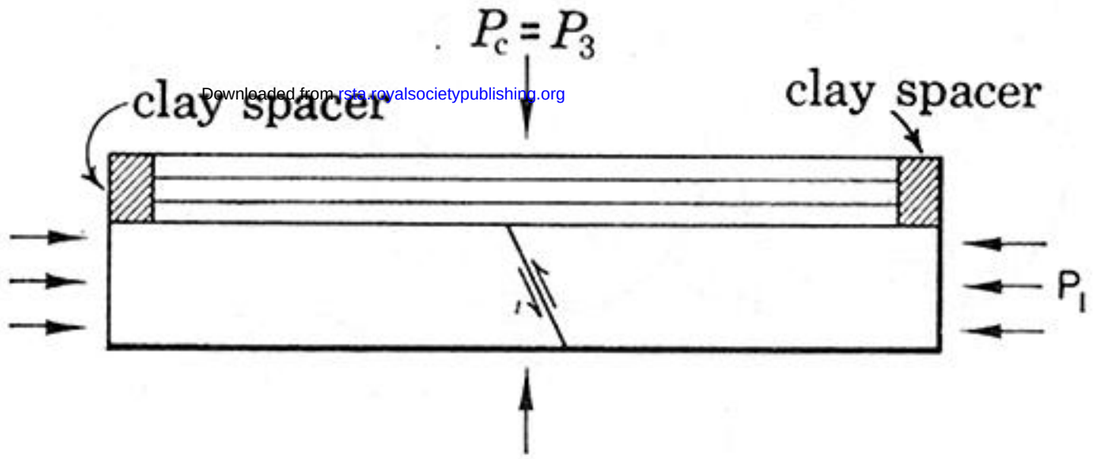

(a)

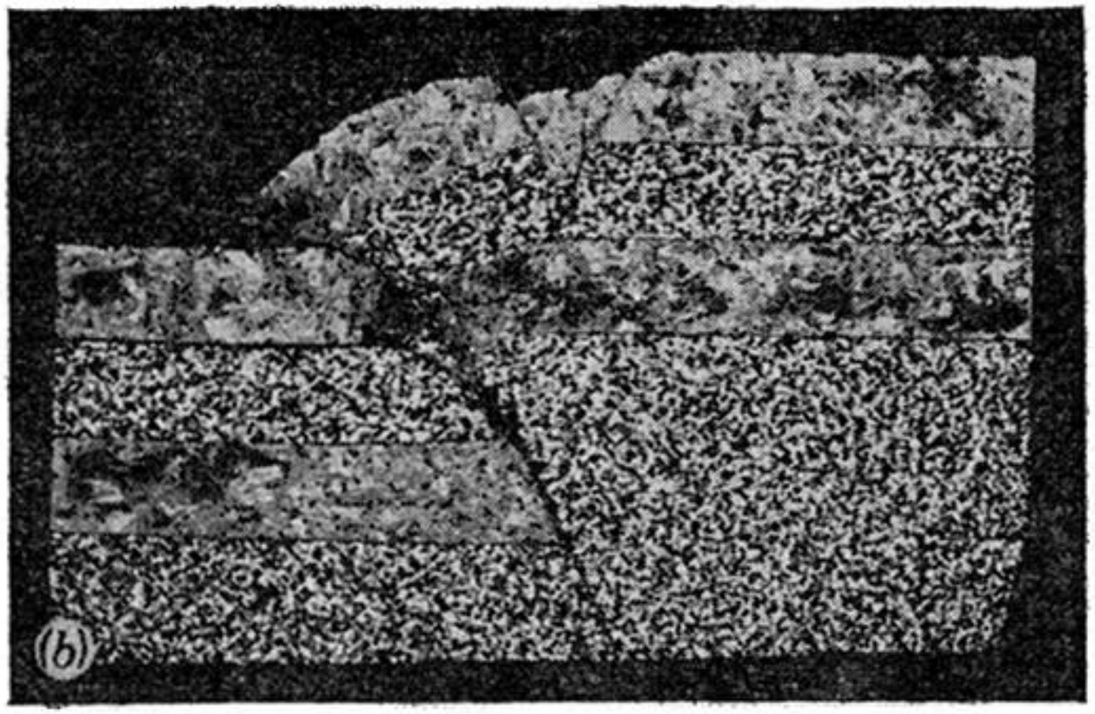

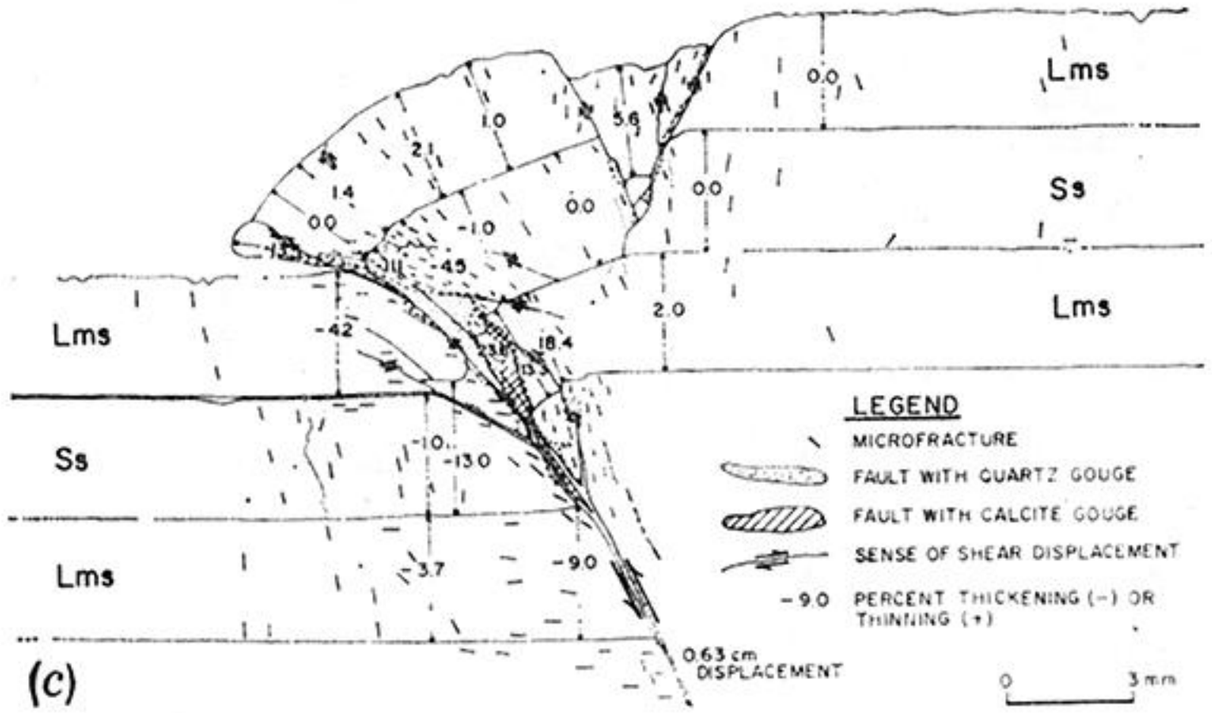

(c)

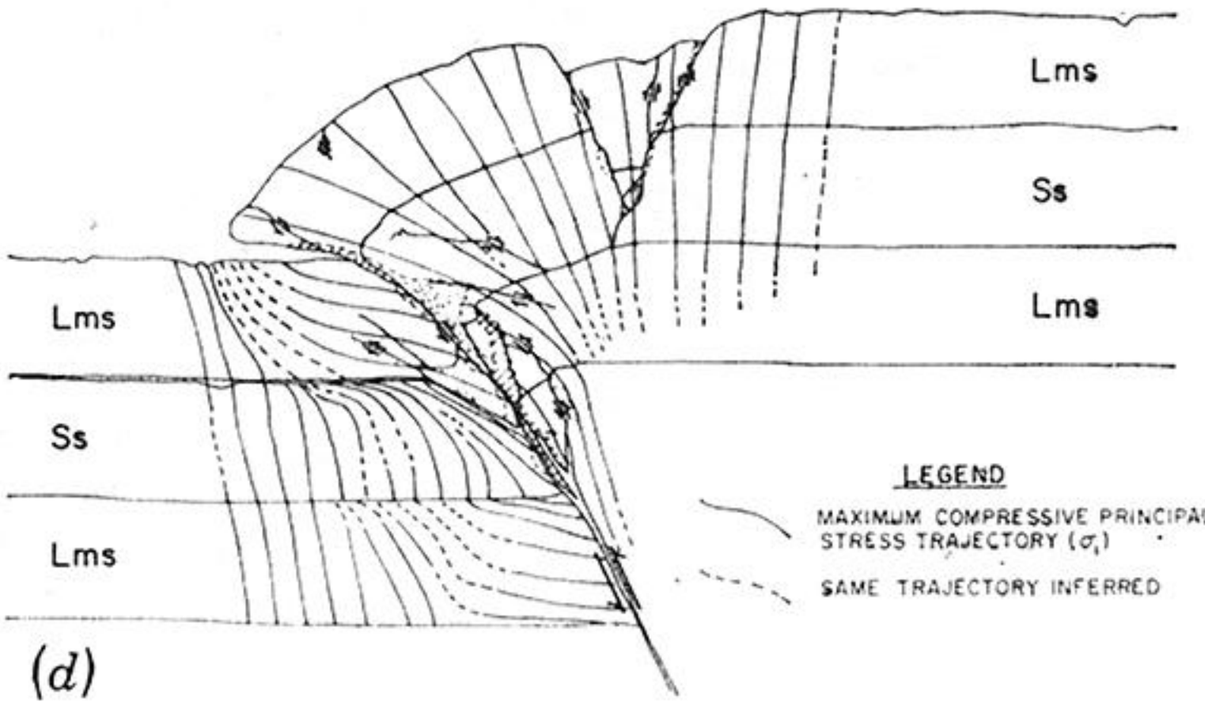

(d)

FIGURE 8. Faulted drape-folds. (*a*) Schematic diagram of loading condition for three layers deformed over a 65° lubricated pre-cut in the forcing member. (*b*) Photomicrograph of specimen 298 shows upthrown forcing block on right with overlying graben in uppermost limestone layer, curving upthrust, and thickened downthrown layers. (*c*) Map of faults and microfractures in specimen 298, also shows strains (percentages) perpendicular to layering as calculated from layer thickness changes, thinnings are positive. (*d*) Stress trajectories inferred from faults, microfractures, and calcite data, specimen 298.